

# HMARK: Radioactive Multi-Bit Semantic-Latent Watermarking for Diffusion Models

Kexin Li<sup>1</sup> Guozhen Ding<sup>1</sup> Ilya Grishchenko<sup>1</sup> David Lie<sup>1</sup>

<sup>1</sup>University of Toronto



Figure 1. Visual comparison between original and watermarked images. Each pair shows the original (left) and watermarked (right) images.

## Abstract

Modern generative diffusion models rely on vast training datasets, often including images with uncertain ownership or usage rights. Radioactive watermarks—marks that transfer to a model’s outputs—can help detect when such unauthorized data has been used for training. Moreover, aside from being radioactive, an effective watermark for protecting images from unauthorized training also needs to meet other existing requirements, such as imperceptibility, robustness, and multi-bit capacity. To overcome these challenges, we propose HMARK, a novel multi-bit watermarking scheme, which encodes ownership information as secret bits in the semantic-latent space ( $h$ -space) for image diffusion models. By leveraging the interpretability and semantic significance of  $h$ -space, ensuring that watermark signals correspond to meaningful semantic attributes, the watermarks embedded by HMARK exhibit radioactivity, robustness to distortions, and minimal impact on perceptual quality. Experimental results demonstrate that HMARK achieves 98.57% watermark detection accuracy, 95.07% bit-level recovery accuracy, 100% recall rate, and 1.0 AUC on images produced by the downstream adversarial model finetuned with LoRA on watermarked data across various types of distortions.

## 1. Introduction

Diffusion models (DMs) produce high-quality photo-realistic images [36, 47, 48, 52, 53]. Such capabilities

are not achievable without training on massive datasets of images. Unfortunately, this hunger for training data means that model builders do not always obtain the necessary consent and authorization to use data. This practice has raised legal and ethical concerns, particularly when the images generated by the trained models closely resemble those of artists and studios, undermining originality and creativity. For instance, Studio Ghibli, renowned for its distinctive animation style, has become a frequent target of stylistic imitation through publicly accessible generative platforms (e.g., OpenAI) [5, 16, 42]. Moreover, methods such as LoRA finetuning [25] and personalization [17, 50] enable a DM to learn an artist’s style (*i.e.*, style transfer) with only a few images. Disputes over whether unauthorized training has taken place and whether the outputs constitute a violation of IP rights have resulted in high-profile lawsuits, such as *Andersen v. Stability AI* and *Getty Images v. Stability AI* [1, 4, 6, 10, 15, 18, 41, 45, 54, 55, 68]. A key consideration in such disputes is proving that unauthorized images were indeed used in the training of the model.

Image *watermarks* are important tools in the arsenal that content producers have to protect their IP against unauthorized training on generative models [34, 37, 70]. Watermarking involves manipulating an image to embed a specially crafted signal (*i.e.*, a watermark). A corresponding detection mechanism can then distinguish between images that contain an embedded watermark and those that do not. Thus, detecting that the output of DM contains a watermark provides strong evidence that the DM trained on watermarked images. For this purpose, a watermark must satisfy four key properties: (1) *robustness*: the watermark should not be removable

\*Under review.

without severely damaging the quality of the watermarked image; (2) *fidelity*: the watermark needs to preserve the perceptual quality of the protected image; (3) *multi-bit capacity*: the watermark should not only be detectable (zero-bit) but also encode ownership information (multi-bit capacity), *e.g.*, to support traitor tracing [7]; and (4) *radioactivity* [11]: the watermark should be present in the output of a DM trained on watermarked images. The last property, in particular, is not sufficiently addressed in the literature.

Existing watermarking schemes can be broadly categorized into three types: pixel-space, modifying the pixels of the image directly; latent-space, modifying the latent space of a trained model; and semantic watermarks, altering generated images in a human-interpretable way. Pixel-space watermarks have been shown to be non-robust and can be easily removed without damage to the image [74]. Similarly, latent-space watermarks can be non-robust and also tend to be non-radioactive if they perturb images in a space that the downstream DM does not learn [11]. In contrast, semantic watermarks aim to introduce a shift in the semantic content of watermarked images [8, 69, 75]. Such watermarks can be radioactive: DMs are trained to capture semantic structures in the data distribution, and therefore are likely to learn and propagate the distribution shift induced by a semantic watermark. However, since these methods do not constrain semantic perturbations, they may substantially modify the image, damaging the fidelity.

We thus propose HMARK—the first *semantic-latent* watermarking scheme that is robust, quality-preserving, multi-bit, and radioactive. HMARK achieves radioactivity by embedding a watermark perturbation in the semantic-latent space, also known as the *h-space*, and achieving the other desired properties by optimizing the perturbation against robustness, fidelity and multi-bit capacity. Embedding the watermark in *h-space* allows HMARK to modify images in a very controlled way to meet these other desired properties, while still maintaining radioactivity *by construction*. In contrast, existing semantic watermarking methods [8, 69] manipulate semantic features in a sub-optimal way, resulting in lower watermark imperceptibility without achieving radioactivity [11]. HMARK is able to optimize its watermark perturbation because we assume that the watermark user can train the perturbation against a representative distribution of images. We observe that this condition is generally met, as the watermark user is usually the content owner.

Semantic-latent operation enables effective training, which balances two opposing objectives—minimization of perceived changes to the protected image and radioactivity resulting from these semantic changes. Remarkably, HMARK achieves radioactivity while introducing only minimally perceptible changes, such as slightly adjusting the age of an individual or subtly altering the individual’s makeup.

In summary, this paper makes the following contributions:

- We present the novel design of the first semantic-latent space watermark, HMARK, which is highly radioactive, while still providing high fidelity, robustness, and multi-bit capacity.
- We evaluate HMARK under diverse distortions, finetuning conditions, and secret-bit configurations to assess its resistance to perturbations, fidelity, and radioactivity.
- HMARK achieves near-perfect watermark detection accuracy, over 95% bit-level secret recovery accuracy, 1.0 AUC, outperforming the state-of-the-art watermarking scheme.

Upon publication, we will make the source code and datasets for HMARK openly available.

## 2. Background

**Diffusion Models.** Diffusion models (DMs) are a class of generative models that have achieved remarkable performance in generating high-quality images, videos, and other modalities. Inspired by concepts from non-equilibrium thermodynamics, DMs consist of two complementary stochastic processes: a *forward diffusion* process, which gradually corrupts input data by adding Gaussian noise until it becomes approximately isotropic Gaussian noise, and a *reverse denoising* process, in which a neural network learns to invert this noising procedure and recover the original data distribution step by step [23, 59–61]. One of the most prevalent and fundamental DMs, Denoising Diffusion Probabilistic Model (DDPM) [23], formulates diffusion as a discrete-time Markov chain, adding noise during the forward pass and iteratively denoising from pure noise back to structured data.

**Interpretable Semantic-latent Space.** Kwon et al. [28] introduced *semantic-latent space* (or *h-space*) of DMs, defined as the collection of UNet [49] bottleneck feature maps across timesteps during the reverse diffusion process. The UNet bottleneck feature maps are the deepest layers of the UNet for each timestep in the reverse denoising process. By design, these feature maps,  $h_t, t \in T..1$ , have the lowest spatial dimensions/resolutions and the most channels/high-level semantics. Therefore, *h-space* is the best place to encode compact and semantically meaningful information and enable semantic edits. *H-space* has three key properties: (1) semantic directions generalize across samples, (2) direction magnitude controls edit strength, and (3) multiple directions can be linearly combined for multi-attribute manipulation. Therefore, *h-space* enables controlled editing of pre-trained DMs in an interpretable manner. For instance, Haas et al. [20] identified semantic directions in *h-space* using Jacobian analysis and PCA, while Park et al. [44] revealed dominant semantics via spectral Jacobian analysis.

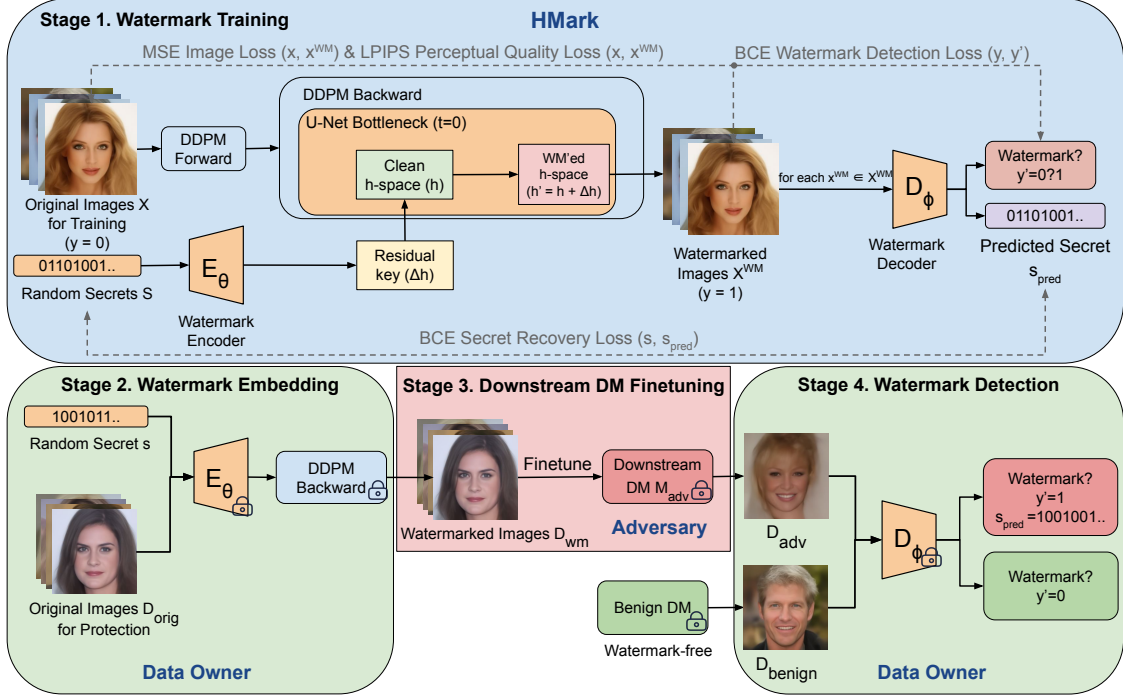


Figure 2. HMARK’s pipeline: (1) HMARK trains a watermarking encoder–decoder on a set of images  $X$  and random secrets; (2) Data owner utilizes HMARK to embed watermarks on their proprietary data  $\mathcal{D}_{\text{orig}}$  for IP protection before publishing; (3) The adversary finetunes  $\mathcal{M}_{\text{adv}}$  on data owner’s watermark-protected  $\mathcal{D}_{\text{wm}}$  scraped online; (4) Data owner utilizes HMARK to detect potential IP infringement in  $\mathcal{D}_{\text{adv}}$ .

### 3. Design of HMARK

#### 3.1. Threat Model

We consider a scenario in which a data owner seeks to protect their proprietary image dataset  $\mathcal{D}_{\text{orig}}$  from unauthorized use in DM finetuning. Our threat model contains three entities: the watermarking technology provider (us), the image dataset owner, and an adversary. To enable copyright protection, the data owner generates the watermarked version of the dataset  $\mathcal{D}_{\text{wm}}$  by embedding imperceptible watermarks into their proprietary images  $\mathcal{D}_{\text{orig}}$ . The adversary controls a DM  $\mathcal{M}_{\text{adv}}$ , obtains an unauthorized copy of the watermarked dataset  $\mathcal{D}_{\text{wm}}$ , and subsequently finetunes their model through incremental training on  $\mathcal{D}_{\text{wm}}$  and generates images  $\mathcal{D}_{\text{adv}}$ . The data owner aims to determine whether the suspect model  $\mathcal{M}_{\text{adv}}$  has been finetuned on  $\mathcal{D}_{\text{wm}}$ . The dataset owner is assumed to have closed-box (API query only) access to the suspect model, allowing them to obtain generated samples  $\mathcal{D}_{\text{adv}}$  but not to inspect the  $\mathcal{M}_{\text{adv}}$ ’s internal parameters.

#### 3.2. Design Overview

We present HMARK, a novel semantic-latent  $h$ -space watermarking scheme. Unlike other types of watermarks, our method trains an autoencoder to discover adaptive semantic embedding that effectively balances the trade-off between watermark imperceptibility and detection robustness. Given

an image  $\mathbf{x} \in \mathbb{R}^{H \times W \times 3}$  and a binary secret watermarking message  $\mathbf{s} \in \{0, 1\}^B$  where  $B$  denotes the secret length, we formulate the watermarking embedding and detection problem as a constrained optimization task. The primary objective involves *embedding*  $\mathbf{s}$  into  $\mathbf{x}$  via a trained  *$h$ -space encoder* to produce a watermarked image  $\mathbf{x}_{\text{wm}}$  while minimizing the perceptual distance  $\|\mathbf{x}_{\text{wm}} - \mathbf{x}\|_2^2$ . Simultaneously, we must train a robust *decoder* that is capable of identifying the presence of the watermark and accurately recovering the embedded secret bits. The scheme additionally requires that the watermark signal remains detectable after exposure to common image transformations and, critically, survives the  $\mathcal{M}_{\text{adv}}$  finetuning processes (*i.e.*, radioactive).

Our methodology, as shown in Figure 2, implements a systematic four-stage pipeline designed to train HMARK and assess whether its watermarks propagate from the unauthorized finetuning data into the learned data distribution, thereby contaminating subsequent samples with detectable watermark traces.

#### 3.3. HMARK’s Training

The training process involves the watermark encoder  $E_\theta$  and decoder  $D_\phi$ , as outlined in the high-level Algorithm 1, Appendix A. In the training process, we apply a custom loss function and distortion-aware input perturbations.

**H-Space Encoder.** The encoder  $E_\theta$  establishes a learnable

transformation that maps discrete binary secrets directly to continuous h-space residuals. The watermark embedding procedure leverages the semantic-preserving properties of the UNet bottleneck layer (h-space) in the reverse diffusion process of DMs. At the final timestep (*i.e.*,  $t = 0$ ) of the reverse diffusion process, the watermark is injected at the UNet bottleneck layer.

$$\begin{aligned} \mathbf{z}_t^{\text{down}} &= \text{DownBlocks}(\mathbf{x}_t, t), \\ \mathbf{h}_t &= \text{MidBlock}(\mathbf{z}_t^{\text{down}}, t) \quad (\text{bottleneck features}), \\ \mathbf{h}_t^{\text{wm}} &= \mathbf{h}_t + \Delta_{\mathbf{h}_t} \quad (\text{additive watermark injection}), \\ \mathbf{x}_{t-1} &= \text{UpBlocks}(\mathbf{h}_t^{\text{wm}}, t). \end{aligned}$$

The encoder  $E_\theta$  is trained to generate residuals  $\Delta_{\mathbf{h}}$  that encode the secret  $\mathbf{s} \in \{0, 1\}^B$  while minimizing perceptual distortion.  $\Delta_{\mathbf{h}}$  is injected into the last timestep of the reverse diffusion and produces watermarked images  $\mathbf{x}_0^{\text{wm}}$ .

**Pixel-Space Decoder.** The detection operates on the image’s pixel space. The decoder identifies the presence of watermarks and recovers the embedded secret message:  $p_{\text{wm}}, \mathbf{s}_{\text{pred}} = D_\phi(\mathbf{x}_{\text{wm}})$  where  $p_{\text{wm}} \in [0, 1]$  is the watermark presence probability (*i.e.*, watermark detected if  $p_{\text{wm}} > 0.5$ ), and  $\mathbf{s}_{\text{pred}} \in \{0, 1\}^B$  is the recovered secret message.  $D_\phi$  incorporates a shared convolutional neural network that learns hierarchical representations optimized for both tasks. This shared representation feeds into task-specific heads, where the detection head performs binary classification and the secret extraction head conducts multi-bit regression.

**Multi-Objective Loss Function.** Our training method employs a multi-objective loss function that addresses the inherent trade-offs between watermark detectability, secret recoverability, and image quality preservation. The multi-component loss function is formulated as:  $\mathcal{L}_{\text{total}} = \lambda_{\text{wm}}\mathcal{L}_{\text{wm}} + \lambda_{\text{secret}}\mathcal{L}_{\text{secret}} + \lambda_{\text{image}}\mathcal{L}_{\text{image}} + \lambda_{\text{lips}}\mathcal{L}_{\text{lips}}$ .

The *watermark detection* loss  $\mathcal{L}_{\text{wm}}$  employs binary cross-entropy (BCE) with logits:

$$\mathcal{L}_{\text{wm}} = -\frac{1}{N} \sum_{i=1}^N [y_i \log \sigma(z_i) + (1 - y_i) \log(1 - \sigma(z_i))],$$

where  $z_i \in \mathbb{R}$  is the decoder’s logit output and  $y_i \in \{0, 1\}$  indicates watermark presence. It optimizes the decoder’s ability to distinguish between watermarked and original images, ensuring reliable watermark presence identification.

The *secret recovery* loss  $\mathcal{L}_{\text{secret}}$  utilizes bit-wise binary cross-entropy to maximize the accuracy of individual bit predictions, improving reconstruction of the embedded secret message. It is computed over watermarked images ( $y_i = 1$ ):

$$\begin{aligned} \mathcal{L}_{\text{secret}} = -\frac{1}{|\mathcal{W}| \cdot B} \sum_{i \in \mathcal{W}} \sum_{j=1}^B & \left[ s_{ij} \log \sigma(z_{ij}) \right. \\ & \left. + (1 - s_{ij}) \log(1 - \sigma(z_{ij})) \right], \end{aligned}$$

where  $B$  is the number of bits,  $s_{ij} \in \{0, 1\}$  is the  $j$ -th bit of the  $i$ -th secret, and  $z_{ij} \in \mathbb{R}$  is the predicted logit.

The *image fidelity* loss  $\mathcal{L}_{\text{image}}$  incorporates mean squared error (MSE) in the pixel space:

$$\mathcal{L}_{\text{image}} = \frac{1}{NCHW} \cdot \sum_{i=1}^N \sum_{c=1}^C \sum_{h=1}^H \sum_{w=1}^W (X_{i,c,h,w}^{\text{wm}} - X_{i,c,h,w})^2,$$

where  $X^{\text{wm}}$  and  $X$  denote the watermarked and original images, respectively.

Finally, the *perceptual quality* loss component  $\mathcal{L}_{\text{lips}}$  leverages LPIPS [72] with normalized inputs to preserve high-level visual characteristics and semantic content:

$$\mathcal{L}_{\text{lips}} = \frac{1}{N} \sum_{i=1}^N \text{LPIPS}(X_i, X_i^{\text{wm}}), \quad X \in [-1, 1].$$

It is important to note that radioactivity is not explicitly included in the loss objective. It is achieved by construction rather than through optimization.

**Distortion-Aware Training.** We apply a diverse set of distortions during the training process, following SleeperMark’s selection [67], which includes additive Gaussian noise, spatial filtering through Gaussian blur convolutions, compression, photometric variations through brightness and contrast adjustments, and geometric transformations via multi-scale resizing. This comprehensive distortion regime operates with a uniform probability throughout training, ensuring that the decoder develops invariance to these perturbations without overfitting to any transformation.

### 3.4. Theoretical Intuition on Radioactivity

HMARK injects watermark information into the UNet bottleneck (h-space), which results in semantic shifts, rather than direct pixel modifications. When a watermark residual  $\Delta_{\mathbf{h}}$  is added in the latent space, all images that embed the same secret receive the same latent shift, even though each image has different pixel-level content. Because the watermark perturbation is constant in h-space, the effect is coherent throughout the dataset. That is, HMARK introduces a shift to the distribution rather than isolated perturbations to individual samples. Diffusion models learn a score function [23], the gradient of the log-density  $\nabla_{\mathbf{x}} \log p(\mathbf{x})$ , which characterizes the data distribution. Thus, a coherent distribution shift in the training data can be reflected in the learned score function. Empirically, we observe that this allows watermark information to persist after finetuning.

Formally, let  $P_{\text{orig}}$  be the original data distribution. Injecting a latent residual modifies the last UNet in the reverse diffusion process as follows, producing the watermarked dataset distribution:

$$T_{\Delta_{\mathbf{h}}}(\mathbf{x}) = \text{UpBlocks}(\mathbf{h} + \Delta_{\mathbf{h}}, 0)$$

$$P_{\text{wm}} = (T_{\Delta_{\mathbf{h}}})_{\#} P_{\text{orig}}.$$

To understand how the latent residual affects the resulting image, we linearize the decoder around each image’s latent bottleneck point. The decoder’s Jacobian  $\mathbf{B}(\mathbf{x})$  maps the change in latent representation to the pixel space:

$$\mathbf{x}^{\text{wm}} \approx \mathbf{x} + \mathbf{B}(\mathbf{x}) \Delta_{\mathbf{h}}, \quad \mathbf{B}(\mathbf{x}) = \left. \frac{\partial \text{UpBlocks}}{\partial \mathbf{h}} \right|_{(\mathbf{h}_0, \mathbf{z}_0^{\text{down}})}.$$

Even though  $\mathbf{B}(\mathbf{x})$  differs for each sample,  $\Delta_{\mathbf{h}}$  is the same for all the images when the same secret is embedded. Aggregated over the dataset, this results in a distribution shift in expectation:

$$\Delta \mu_x := \mathbb{E}_{P_{\text{wm}}}[\mathbf{x}] - \mathbb{E}_{P_{\text{orig}}}[\mathbf{x}] \approx \left( \mathbb{E}_{\mathbf{x} \sim P_{\text{orig}}}[\mathbf{B}(\mathbf{x})] \right) \Delta_{\mathbf{h}}.$$

When the downstream model trains on a watermarked dataset  $\mathcal{D}_{\text{wm}}$ , the model learns the watermarked score function. As a result, the generation of the downstream model converges to the modified distribution,  $\hat{P}^{\text{gen}} \approx P_{\text{wm}}$ . This provides an intuition as to why watermarks embedded by HMARK are radioactive by construction, as they embed their signals into the dataset distribution which is later learned by the downstream model.

## 4. Evaluation

In this section, we discuss experiments on HMARK, evaluating its radioactivity, robustness, imperceptibility, and capacity. All experiments are performed on a machine with two Intel Xeon Gold 6548Y processors and four Nvidia H100 GPUs having 96GB of high-bandwidth memory.

**Models and Dataset.** At Stages 1 and 2 (*i.e.*, HMARK’s training and embedding in Figure 2), we use the h-space-enabled semantic DDPM [20] for watermark injection. At Stages 3 and 4, we employ a pixel-space DDPM [23] as the attacker’s  $\mathcal{M}_{\text{adv}}$ . To ensure a closed-box setting, we use a pre-trained model checkpoint google/ddpm-celebahq-256 on the CelebA-HQ dataset [32]. The finetuning techniques we adapt are the basic DDPM’s UNet finetuning and LoRA (rank = 8, 16, 32) [25]. We use finetuning scripts from Hugging Face Diffusers’ official GitHub repository [65] with minimal changes to support DDPM. Due to space constraints, we present the results on LoRA in this section, and the UNet finetuning results are discussed in Appendices D, J and K.

At Stage 1, to train HMARK, we use 100,000 generated images from the semantic DDPM with random secret bits under different random seeds. At Stage 2, we use a protected dataset  $\mathcal{D}_{\text{orig}}$  (see Section 3.1) of 10,000 samples to generate a  $\mathcal{D}_{\text{wm}}$ . Note that  $\mathcal{D}_{\text{orig}}$  is not part of our training dataset, thereby ensuring generalizability. At Stage 3, the adversary uses  $\mathcal{D}_{\text{wm}}$  to finetune  $\mathcal{M}_{\text{adv}}$ . At Stage 4, we evaluate HMARK’s detector’s effectiveness in distinguishing  $\mathcal{D}_{\text{adv}}$

(*i.e.*, outputs of  $\mathcal{M}_{\text{adv}}$ ) from  $\mathcal{D}_{\text{benign}}$  (*i.e.*, outputs of a benign downstream DM without finetuning). We study the impact of the size of  $\mathcal{D}_{\text{wm}}$ ,  $|\mathcal{D}_{\text{wm}}|$ , in Section 4.1.

Although in our threat model, the adversary cannot acquire  $\mathcal{D}_{\text{orig}}$  (*i.e.*, the same dataset as  $\mathcal{D}_{\text{wm}}$  but watermark-free) and thus cannot generate  $\mathcal{D}_{\text{clean}}$  (*i.e.*, outputs of a downstream DM finetuned on  $\mathcal{D}_{\text{orig}}$ ), we still evaluate HMARK’s effectiveness to distinguish  $\mathcal{D}_{\text{adv}}$  from  $\mathcal{D}_{\text{clean}}$ . This evaluation allows us to compute the false positive rate of HMARK, and confirm the authenticity of its detection results.

In evaluation, finetuning is 9,000-step, which is selected based on examples in Hugging Face Diffusers module [12, 65]. We analyze the effect of the number of finetuning steps in Section 4.5. Other training and finetuning hyperparameter choices are presented in Appendix B. Although the evaluation focuses on embedding 8-bit secrets, we also study HMARK’s support of different secret sizes, and results are discussed in Section 4.4.

**Evaluation Metrics and Comparison.** We evaluate HMARK’s effectiveness using watermark detection accuracy,  $\text{Acc}_{\text{WM}} = \frac{TP+TN}{TP+TN+FP+FN}$ ; bit-level secret accuracy,  $\text{Acc}_{\text{bit}} = \frac{1}{B} \sum_{j=1}^B [\hat{s}_j = s_j]$ , where  $s_j$  is the  $j$ -th index of the ground-truth secret  $\mathbf{s}$  and  $\hat{s}_j$  is the  $j$ -th index of the predicted secret  $\hat{\mathbf{s}}$  by the detector,  $\mathbf{s}, \hat{\mathbf{s}} \in \{0, 1\}^B$ ; precision,  $P = \frac{TP}{TP+FP}$ ; recall rate,  $R = \frac{TP}{TP+FN}$ ; and F1 score,  $F_1 = 2 \times \frac{P \times R}{P+R}$ . We also use Receiver Operating Characteristic (ROC) and Area Under the Curve (AUC) [3]. We quantitatively measure visual fidelity using Mean Squared Error (MSE) [39], Structural Similarity Index (SSIM) [66], Learned Perceptual Image Patch Similarity (LPIPS) with AlexNet [72], and Fréchet Inception Distance (FID) [22].

Table 1. Evaluation of HMARK’s effectiveness, compared to Recipe watermarking scheme [75]. Stage 2 results show the immediate post-embedding watermark effectiveness, while Stage 4 results show HMARK’s radioactivity across finetuning methods.

Stg.	Scheme	Finetune	$\text{Acc}_{\text{WM}}$ (%)	$\text{Acc}_{\text{bit}}$ (%)	P (%)	R (%)	F1 (%)
2	Recipe	NA	99.3	57.2	98.6	100.0	99.3
	HMARK	NA	99.0	97.4	98.1	100.0	99.1
4	Recipe	UNet	50.8	16.7	72.4	2.7	5.2
		LoRA	50.6	16.1	77.2	2.0	3.9
	HMARK	UNet	98.1	87.4	97.3	99.0	98.2
		LoRA	98.6	95.1	97.2	100.0	98.6

### 4.1. Effectiveness and Radioactivity

To evaluate HMARK’s effectiveness, we collect the results from two detection points: (1) watermarked images ( $\mathcal{D}_{\text{wm}}$ ) generated from stage 2, and (2) generated outputs ( $\mathcal{D}_{\text{adv}}$ ) from the adversary’s  $\mathcal{M}_{\text{adv}}$  at stage 4. We compare HMARK with a well-known watermarking scheme *Recipe* [75]. We select *Recipe* as it is the only recent DDPM-supporting watermark we are aware of at the time of writing.

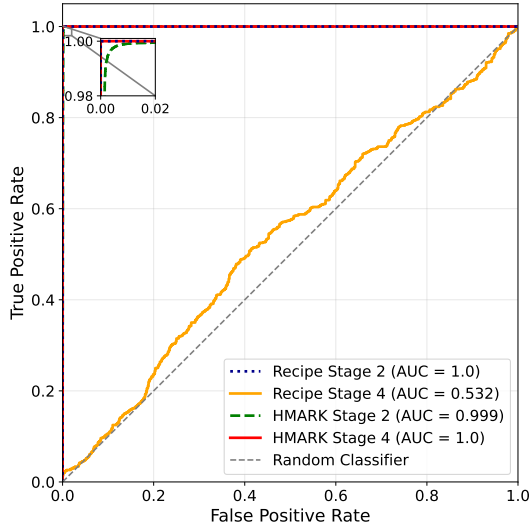


Figure 3. ROC curves of Recipe versus HMARK at Stage 2 and Stage 4 when  $\mathcal{M}_{adv}$  is LoRA finetuned.

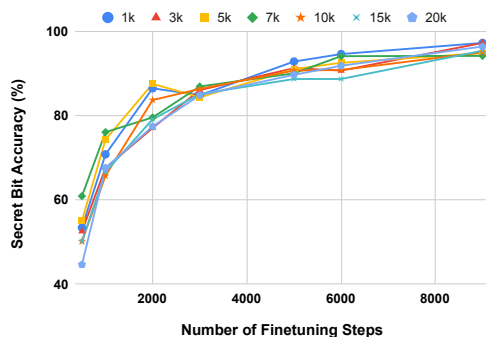


Figure 4. Impact of  $|\mathcal{D}_{wm}|$  on  $\text{Acc}_{bit}$  and the evolution of HMARK’s performance as the number of finetuning steps increases when  $\mathcal{M}_{adv}$  is LoRA finetuned.

Table 1 presents Recipe and HMARK’s watermark performances when 8-bit secrets are embedded. Tested on  $\mathcal{D}_{wm}$  and  $\mathcal{D}_{orig}$ , both HMARK and Recipe achieve high  $\text{Acc}_{wm}$  of around 99%, but HMARK excels at secret recovery with  $\text{Acc}_{bit}$  of 97.4% versus Recipe’s 57.2%.

After  $\mathcal{M}_{adv}$  finetuning, evaluated on 100 samples from  $\mathcal{D}_{adv}$  and 100 samples from  $\mathcal{D}_{benign}$ ,  $\text{Acc}_{wm}$  still remains near-perfect for HMARK, demonstrating the radioactivity of the embedded watermark. The consistently high  $\text{Acc}_{bit}$  (87.43% with UNet finetuning and 95.07% with LoRA rank = 32) and F1 scores further confirm HMARK’s robustness and reliability across adversarial settings. We also study the effect of LoRA ranks and discuss the results of lower ranks (16 and 8) in Appendix F. We observe that HMARK’s  $\text{Acc}_{bit}$  can exceed 95% for all the ranks.

In contrast, Recipe’s  $\text{Acc}_{wm}$  drops to almost 50% for

both finetuning techniques. Based on the ROC analysis in Figure 3, we observe that at Stage 2, both schemes demonstrate excellent  $\text{Acc}_{wm}$  with AUC values of 0.999 and 1.0, respectively. At Stage 4, however, HMARK maintains its reliable detection capability with an AUC of 1.0, whereas Recipe exhibits substantial degradation (*i.e.*, AUC drops to 0.532), barely exceeding random guessing.

To further verify HMARK’s detection authenticity and robustness against false attribution, we evaluate its behavior on 200 generated outputs  $\mathcal{D}_{clean}$  that were not watermarked. HMARK achieves 93.93%  $\text{Acc}_{wm}$  with 6.07% FPR and 30.27%  $\text{Acc}_{bit}$ . These results demonstrate that HMARK reliably identifies almost all outputs of  $\mathcal{M}_{adv}$  as unwatermarked, even though the underlying training images are identical to those of  $\mathcal{D}_{wm}$  but without watermarks. Although a small fraction of benign samples are mistakenly flagged as watermarked, the 30.27%  $\text{Acc}_{bit}$  confirms that HMARK cannot extract any valid secret bits from them, thereby validating the watermark’s detection authenticity. Detailed results for different distortions are in Table 5 in Appendix C. Detailed evaluation results for Recipe are presented in Appendix E.

As shown in Figure 4, HMARK’s effectiveness is relatively insensitive to the number of watermarked images  $|\mathcal{D}_{wm}|$ . HMARK is highly reliable in watermark detection even when  $|\mathcal{D}_{wm}|$  is as *small* [51] as 1,000, with  $\text{Acc}_{wm}$  constantly around 98.5% for all  $\mathcal{D}_{wm}$  sizes. Figure 4 also confirms the theoretical intuition (Section 3.4)— $\text{Acc}_{bit}$  improves, as the model becomes better at understanding the finetuning distribution with each step.

Overall, the results indicate that HMARK is radioactive and reliable in watermark detection. Detailed results are presented in Table 14 in Appendix I.

Table 2. Performance of HMARK evaluated on  $\mathcal{M}_{adv}$ ’s generated outputs ( $\mathcal{D}_{adv}$ ) at Stage 4 under different distortions.  $\mathcal{M}_{adv}$  is trained with LoRA finetuning script (rank = 32).

Distortion	$\text{Acc}_{wm}$ (%)	$\text{Acc}_{bit}$ (%)	P (%)	R (%)	F1 (%)
Identity	99.00	94.00	98.04	100.00	99.01
Gaussian Noise	99.00	95.75	98.04	100.00	99.01
Brightness	98.50	94.38	97.09	100.00	98.52
Contrast	99.00	94.50	98.04	100.00	99.01
Blur	98.50	95.50	97.09	100.00	98.52
JPEG	99.00	95.25	98.04	100.00	99.01
Resize	97.00	97.12	94.34	100.00	97.09
<b>Average</b>	<b>98.57</b>	<b>95.07</b>	<b>97.22</b>	<b>100.00</b>	<b>98.59</b>

## 4.2. Robustness

To evaluate HMARK’s resistance to common image distortions, we simulate a range of realistic perturbations, whose parameter settings are provided in Appendix D. These distortions emulate both intentional post-processing edits and natural image degradations that may occur during acquisi-

tion, compression, or transmission in real-world scenarios. Specifically, we consider six types of perturbations: Gaussian noise addition, brightness adjustment, contrast variation, blurring, JPEG compression, and resizing [67].

Table 2 demonstrates that HMARK consistently achieves near-perfect  $\text{Acc}_{\text{WM}}$ , high  $\text{Acc}_{\text{bit}}$ , and a 100% recall rate, regardless of common perturbations applied to the outputs of  $\mathcal{M}_{\text{adv}}$ . These results confirm HMARK’s radioactivity.

Stage 2 results (high  $\text{Acc}_{\text{WM}}$  and  $\text{Acc}_{\text{bit}}$ ) are shown in Table 6 in Appendix D. Comparative analyses of HMARK across different finetuning scripts and secret bit lengths are provided in Appendices D and J.

Table 3. Fidelity metrics for different secret bit configurations collected on 10,000 (clean, watermarked) image pairs. ( $\pm$  represents the standard deviation). Lower is better for MSE, LPIPS, and FID; higher is better for SSIM. Result for Recipe is tested on 8-bit secret.

# Bits	MSE ( $\downarrow$ )	SSIM ( $\uparrow$ )	LPIPS ( $\downarrow$ )	FID ( $\downarrow$ )
Recipe	$2.47\text{e-}4 \pm 3.5\text{e-}5$	$0.9747 \pm 0.0035$	$0.141 \pm 0.0417$	30.4025
8	$1.49\text{e-}4 \pm 6.8\text{e-}5$	$0.9725 \pm 0.0046$	$0.0511 \pm 0.0155$	8.3161
16	$1.72\text{e-}4 \pm 9.1\text{e-}5$	$0.9683 \pm 0.0056$	$0.0605 \pm 0.0182$	7.6229
32	$1.38\text{e-}4 \pm 9.6\text{e-}5$	$0.9740 \pm 0.0044$	$0.0472 \pm 0.0149$	6.8820

### 4.3. Fidelity

We evaluate watermark fidelity and invisibility in Table 3. Overall, images with watermarks  $\mathcal{D}_{\text{wm}}$  exhibit high perceptual quality and imperceptibility. Representative examples are shown in Figure 1 and Figure 5 in Appendix G.

The pixel-level distortion, measured by MSE, remains low (on the order of  $10^{-4}$ ) with small variance across secret bit lengths, indicating negligible embedding artifacts. SSIM measures the structural similarity by considering, among other metrics, luminance, contrast, and structural components.  $\mathcal{D}_{\text{wm}}$ ’s SSIM values are over 96%, indicating that the structural and perceptual content of the images remains highly consistent after watermarking. LPIPS leverages deep neural network features to measure perceptual differences between image pairs (*i.e.*, 0 indicates identical perception). In our case, we obtain favorable LPIPS scores (0.04–0.06), indicating that  $\mathcal{D}_{\text{wm}}$  are perceptually indistinguishable from  $\mathcal{D}_{\text{orig}}$ . Lastly, FID evaluates the distributional similarity between real and generated (in our case,  $\mathcal{D}_{\text{orig}}$  and  $\mathcal{D}_{\text{wm}}$ ). Our FID scores (6.9–8.3) demonstrate that the overall distribution and fidelity of the images are well preserved. Compared to Recipe, HMARK’s watermarked image fidelity is comparable in SSIM and substantially better in other metrics.

Notably, these metrics are consistent across 8-, 16-, and 32-bit secrets, suggesting that watermark imperceptibility is insensitive to embedding capacity. Figure 6 in Appendix H presents images generated from  $\mathcal{M}_{\text{adv}}$  finetuned on  $\mathcal{D}_{\text{orig}}$ ,  $\mathcal{D}_{\text{wm}}$  with 8-bit secret,  $\mathcal{D}_{\text{wm}}$  with 16-bit secret, and  $\mathcal{D}_{\text{wm}}$  with 32-bit secret. As finetuning progresses, outputs appear

more natural, making it harder for an adversary to distinguish clean from watermarked images.

Table 4. HMARK’s performance on radioactivity to  $\mathcal{M}_{\text{adv}}$  finetuned with LoRA ( $\text{rank} = 32$ ) with different secret bit lengths.

# Bits	$\text{Acc}_{\text{WM}}$ (%)	$\text{Acc}_{\text{bit}}$ (%)	P (%)	R (%)	F1 (%)
8	98.57	95.07	97.22	100.00	98.59
16	99.50	93.73	99.43	99.14	99.50
32	90.71	68.70	87.88	94.57	91.04

### 4.4. Secret Size Analysis

Supporting increasing secret sizes is important as it allows assigning exponentially more unique identifiers to watermark users. Table 4 shows HMARK’s performance averaged across various distortions when different secret sizes (8, 16, 32 bits) are embedded and transmitted during downstream DDPM finetuning with LoRA.

Following our theoretical intuition (Section 3.4), as more information is communicated through the distribution shift with HMARK, it becomes harder for the downstream DM to learn this shift. Thus, the recovery degrades as the secret size grows with the same number of finetuning steps. Results in Table 4 confirm this theoretical intuition. HMARK achieves 95.07% and 93.73%  $\text{Acc}_{\text{bit}}$  when the secret size is 8 and 16 bits, respectively, and, as we double the secret size to 32,  $\text{Acc}_{\text{bit}}$  drops to 68.70%. To improve these results, even when the number of finetuning steps is limited, HMARK supports Bose-Chaudhuri-Hocquenghem (BCH) error correction code [2], which helps HMARK to achieve  $\text{Acc}_{\text{bit}}$  of above 90%. See details in Appendix L.

Notably, with growing secret sizes,  $\text{Acc}_{\text{WM}}$  decreases only gradually (from 99.50% to 90.71%), precision and recall remain high, showing that HMARK maintains reliable watermark detectability even at larger bit lengths. Detailed tabularized results on LoRA and default UNet finetuning are presented in Appendix J.

### 4.5. Relationship of $\text{Acc}_{\text{bit}}$ and Finetuning

For most part of the evaluation, we set the finetuning step count to 9,000, following Hugging Face Diffusers’ GitHub sample configurations [65]. However, we also analyze how HMARK’s performance evolves during finetuning, recording evaluation metrics at several step configurations, ranging from 500 to 30,000 steps.

When  $\mathcal{M}_{\text{adv}}$  is trained using LoRA (*i.e.*, for  $\text{rank} = 8, 16, 32$ ), we observe that higher ranks yield strong watermark detection early on. For example, with  $\text{rank} = 32$ ,  $\text{Acc}_{\text{WM}}$  starts at 94.21% at step 500, surpasses 96% soon after, and exceeds 98% beyond 4,000 steps. Meanwhile,  $\text{Acc}_{\text{bit}}$  improves more gradually—remaining under 80% before 2,000 steps, crossing 90% around 4,000 steps, and reaching over 95% by 9,000 steps. This trend suggests that HMARK

maintains high  $\text{Acc}_{\text{WM}}$  regardless of the duration of  $\mathcal{M}_{\text{adv}}$ 's finetuning. Additional training mainly boosts  $\text{Acc}_{\text{bit}}$ , but the improvement quickly saturates at a relatively modest level, indicating diminishing returns beyond approximately 6k–9k steps. A similar trend is observed when  $\mathcal{M}_{\text{adv}}$  is finetuned with default UNet script. Here,  $\text{Acc}_{\text{WM}}$  stays above 97% throughout, confirming stable watermark detectability, while  $\text{Acc}_{\text{bit}}$  gradually rises before leveling off after 6,000 steps. Specifically, HMARK achieves around 61%  $\text{Acc}_{\text{bit}}$  within the first 3,000 steps, increases to 81.86% after 5,000 steps, and surpasses 85% beyond 6,000 steps, eventually reaching 87.64% at 30,000 steps. Tabularized results are presented in Tables 17 and 18 in Appendix K.

## 5. Limitations

Although HMARK achieves radioactivity agnostically to the finetuning method (LoRA and default UNet finetuning) [25, 65], finetuning algorithms with latent-space diffusion process such as Latent Diffusion Models (LDMs) [48] may require additional training. While we acknowledge this limitation, it is orthogonal to our main contribution, which is a multi-bit semantic-latent space watermarking scheme that is high-fidelity, robust and radioactive by construction.

## 6. Related Work

**Watermarking.** Watermarking schemes are widely used for IP protection and ownership verification. Watermarks have been injected into Convolutional Neural Networks using feature-domain patterns [33], colour-space triggers [26], and architectural backdoors [29]. While effective for classification tasks with discrete outputs, these methods struggle in generative settings, where outputs are continuous and high-dimensional, making consistent trigger responses unreliable. Generative adaptations such as [58] show promise but remain vulnerable to removal attacks [24]. Latent-space watermarking approaches, such as WaDiff [38], PRC [19] and Stable Signature [13], embed watermarks directly into the generative process. However, these methods still face the challenge of achieving radioactivity [11], ensuring all outputs from the downstream model carry the watermark. Invisible pixel-space watermarks [46, 63, 71] are provably removable using generative AI [74], motivating semantic watermarks that modify high-level content while preserving meaning. Examples include Tree-Ring [69], which embeds patterns in the initial noise vector, and RingID [8], which extends this idea to multi-bit capacity. SleeperMark [67] takes a different approach, disentangling watermark information from semantics to survive DM finetuning. As for [35], although it is radioactive, its watermarks are only zero-bit.

**Cloaking.** Cloaking schemes share a similar goal with ours, offering an alternative means of protecting datasets and preventing unauthorized model training through adver-

sarial redirection. Glaze [57] applies imperceptible “style cloaks” that mislead models attempting to imitate an artist’s style. MetaCloak [31] uses meta-learning to generate transferable perturbations robust to transformations, while Anti-Dreambooth [30] disrupts personalized text-to-image finetuning via targeted noise. NightShade [56] further introduces perturbations that both cloak and poison, causing DMs trained on protected data to yield corrupted outputs. Despite their promise, cloaking methods face key limitations. They require proactive protection of every image, and their perturbations can be neutralized by standard pre-processing or robust training [14]. Once disclosed, the perturbation algorithm allows for removal and indefinite reuse of the original data, rendering protection ineffective [14]. Moreover, cloaking offers no mechanism for ownership verification or proof of unauthorized use. In contrast, our approach develops a robust, radioactive watermarking scheme operating in the semantic-latent space of DMs to enable verifiable dataset ownership and reliable detection of misuse.

**Data Poisoning.** Data poisoning is a related yet orthogonal research direction to our work. Poisoning attacks aim to maliciously manipulate training data to alter model behavior, degrade performance, or implant backdoors, hence, compromising model integrity and reliability [73]. Recent works highlight the diversity of poisoning strategies and threat models, from label flip and feature injection to stealthy clean-label poisoning [9, 40]. Modern approaches in generative model data poisoning can perturb diffusion and image-generation pipelines through bilateral effects or optimization-based attacks [21, 43, 62]. Although a watermarking scheme has a similar technical idea to data poisoning, it serves a protective role by embedding imperceptible yet verifiable signatures into data to establish ownership or trace unauthorized use, without adversarially degrading model’s utility.

## 7. Conclusion

The rapid innovations of generative DMs have amplified the tension between human creativity, IP rights, and generative AI technologies. Existing watermarking schemes fall short in reliably identifying unauthorized model finetuning on proprietary datasets. To address this critical gap, we introduce HMARK, a novel multi-bit semantic-latent watermarking scheme. HMARK’s watermarks are radioactive, imperceptible, multi-bit, and robust. By embedding semantically meaningful and persistent signals within finetuning data, HMARK enables transparent ownership verification on generated outputs of the downstream models, exceeding 98% watermark detection accuracy, 95% secret bit recovery rate, and perfect AUC, while preserving visual fidelity. Comprehensive evaluation demonstrates HMARK’s effectiveness under diverse distortions and finetuning settings. Together, these advances represent a crucial step towards responsible and legally compliant generative AI development.

## References

- [1] Associated Press. Studio ghibli ai art raises concerns as chatgpt mimics miyazaki’s style. <https://apnews.com/article/studio-ghibli-chatgpt-images-hayao-miyazaki-openai-0f4cb487ec3042dd5b43ad47879b91f4>, 2024. 1
- [2] R. C. Bose and D. K. Ray-Chaudhuri. On a class of error correcting binary group codes. *Information and Control*, 3(1):68–79, 1960. 7, 16
- [3] Andrew P. Bradley. The use of the area under the roc curve in the evaluation of machine learning algorithms. *Pattern Recognition*, 30(7):1145–1159, 1997. 5
- [4] Blake Brittain. Getty images lawsuit says stability ai misused photos to train ai. *Reuters*, 2023. 1
- [5] Bylo AI. Ghibli ai generator: Turn your photos into studio ghibli style art. <https://bylo.ai/features/ghibli-ai>, 2025. 1
- [6] Kelvin Chan. Getty images sues stability ai, alleging unauthorized use of copyrighted photos. *AP News*, 2023. 1
- [7] Benny Chor, Amos Fiat, and Moni Naor. Tracing traitors. In *Annual international cryptology conference*, pages 257–270. Springer, 1994. 2
- [8] Hai Ci, Pei Yang, Yiren Song, and Mike Zheng Shou. Ringid: Rethinking tree-ring watermarking for enhanced multi-key identification, 2024. 2, 8
- [9] Antonio Emanuele Cinà, Kathrin Grosse, Ambra Demontis, Sebastiano Vascon, Werner Zellinger, Bernhard A. Moser, Alina Oprea, Battista Biggio, Marcello Pelillo, and Fabio Roli. Wild patterns reloaded: A survey of machine learning security against training data poisoning. *ACM Computing Surveys*, 55(13s):1–39, 2023. 8
- [10] Legal Dive. Nvidia, openai face youtube creator lawsuits for using online videos. <https://www.legaldive.com/news/nvidia-open-ai-face-youtube-creator-lawsuits-for-using-online-videos/724498/>, 2024. 1
- [11] Jan Dubiński, Michel Meintz, Franziska Boenisch, and Adam Dziedzic. Are Watermarks For Diffusion Models Radioactive? In *The 1st Workshop on GenAI Watermarking*, 2025. 2, 8
- [12] Hugging Face. Lora (low-rank adaptation) — diffusers training guide. <https://huggingface.co/docs/diffusers/training/lora>, 2025. Accessed: 2025-10-29. 5
- [13] Pierre Fernandez, Guillaume Couairon, Hervé Jégou, Matthijs Douze, and Teddy Furon. The stable signature: Rooting watermarks in latent diffusion models. In *Proceedings of the IEEE/CVF International Conference on Computer Vision (ICCV)*, pages 22466–22477, 2023. 8
- [14] Hanna Foerster, Sasha Behrouzi, Phillip Rieger, Murtuza Jadliwala, and Ahmad-Reza Sadeghi. Lightshed: defeating perturbation-based image copyright protections. In *Proceedings of the 34th USENIX Conference on Security Symposium, USA*, 2025. USENIX Association. 8
- [15] Center for Art Law. Artificial intelligence and artists’ intellectual property: Unpacking copyright infringement allegations in andersen v. stability ai ltd. <https://itsartlaw.org/2024/02/26/artificial-intelligence-and-artists-intellectual-property-unpacking-copyright-infringement-allegations-in-andersen-v-stability-ai-ltd/>, 2024. 1
- [16] Fotor. Studio ghibli filter: Ai art generator for ghibli-style images. <https://www.fotor.com/features/studio-ghibli-filter/>, 2025. 1
- [17] Rinon Gal, Yuval Alaluf, Yuval Atzmon, Or Patashnik, Amit H. Bermano, Gal Chechik, and Daniel Cohen-Or. An Image is Worth One Word: Personalizing Text-to-Image Generation using Textual Inversion, 2022. 1
- [18] Getty Images International. Getty images v. stability ai complaint. <https://copyrightalliance.org/wp-content/uploads/2023/02/Getty-Images-v.-Stability-AI-Complaint.pdf>, 2023. 1
- [19] Sam Gunn, Xuandong Zhao, and Dawn Song. An undetectable watermark for generative image models, 2025. 8
- [20] René Haas, Inbar Huberman-Spiegelglas, Rotem Mulayoff, Stella Graßhof, Sami S. Brandt, and Tomer Michaeli. Discovering Interpretable Directions in the Semantic Latent Space of Diffusion Models, 2024. 2, 5
- [21] Pengfei He, Han Xu, Jie Ren, Yingqian Cui, Hui Liu, Charu C. Aggarwal, and Jiliang Tang. Sharpness-aware data poisoning attack, 2025. 8
- [22] Martin Heusel, Hubert Ramsauer, Thomas Unterthiner, Bernhard Nessler, and Sepp Hochreiter. Gans trained by a two time-scale update rule converge to a local nash equilibrium. In *Advances in Neural Information Processing Systems (NeurIPS)*, pages 6626–6637, 2017. 5
- [23] Jonathan Ho, Ajay Jain, and Pieter Abbeel. Denoising Diffusion Probabilistic Models. In *Advances in Neural Information Processing Systems*, pages 6840–6851. Curran Associates, Inc., 2020. 2, 4, 5
- [24] Aoting Hu, Yanzhi Chen, Renjie Xie, and Adrian Weller. On the weaknesses of backdoor-based model watermarking: An information-theoretic perspective, 2024. 8
- [25] Edward J. Hu, Yelong Shen, Phillip Wallis, Zeyuan Allen-Zhu, Yuanzhi Li, Shean Wang, Lu Wang, and Weizhu Chen. LoRA: Low-Rank Adaptation of Large Language Models, 2021. 1, 5, 8
- [26] Wenbo Jiang, Hongwei Li, Guowen Xu, and Tianwei Zhang. Color backdoor: A robust poisoning attack in color space. In *2023 IEEE/CVF Conference on Computer Vision and Pattern Recognition (CVPR)*, pages 8133–8142, 2023. 8
- [27] Jeff Kent. python-bchlib: BCH library C Python module. <https://github.com/jkent/python-bchlib>, 2018. 16
- [28] Mingi Kwon, Jaeseok Jeong, and Youngjung Uh. Diffusion models already have a semantic latent space, 2023. 2
- [29] Harry Langford, Iliia Shumailov, Yiren Zhao, Robert Mullins, and Nicolas Papernot. Architectural neural backdoors from first principles, 2024. 8
- [30] Thanh Van Le, Hao Phung, Thuan Hoang Nguyen, Quan Dao, Ngoc Tran, and Anh Tran. Anti-DreamBooth: Protecting users from personalized text-to-image synthesis, 2023. 8
- [31] Yixin Liu, Chenrui Fan, Yutong Dai, Xun Chen, Pan Zhou, and Lichao Sun. Metacloak: Preventing unauthorized subject-

- driven text-to-image diffusion-based synthesis via meta-learning, 2024. 8
- [32] Ziwei Liu, Ping Luo, Xiaogang Wang, and Xiaoou Tang. Deep learning face attributes in the wild. In *Proceedings of the IEEE International Conference on Computer Vision (ICCV)*, 2015. 5
- [33] Zeyan Liu, Fengjun Li, Zhu Li, and Bo Luo. Loneneuron: A highly-effective feature-domain neural trojan using invisible and polymorphic watermarks. In *Proceedings of the 2022 ACM SIGSAC Conference on Computer and Communications Security*, page 2129–2143, New York, NY, USA, 2022. Association for Computing Machinery. 8
- [34] H. Luo, Y. Zhang, X. Chen, and L. Wang. Digital watermarking technology for ai-generated images. *Mathematics*, 13(4): 651, 2025. 1
- [35] Michel Meintz, Jan Dubiński, Franziska Boenisch, and Adam Dziedzic. Radioactive watermarks in diffusion and autoregressive image generative models, 2025. 8
- [36] MidJourney, Inc. Midjourney. <https://www.midjourney.com>, 2024. 1
- [37] Rui Min, Sen Li, Hongyang Chen, and Minhao Cheng. A watermark-conditioned diffusion model for ip protection, 2024. 1
- [38] Rui Min, Sen Li, Hongyang Chen, and Minhao Cheng. A watermark-conditioned diffusion model for ip protection, 2024. 8
- [39] Alexander M. Mood, Franklin A. Graybill, and Duane C. Boes. *Introduction to the Theory of Statistics*. McGraw-Hill, 3rd edition, 1974. Used as a reference for the Mean Squared Error (MSE) metric. 5
- [40] Thanh Toan Nguyen, Quoc Viet Hung Nguyen, Thanh Tam Nguyen, Thanh Trung Huynh, Thanh Thi Nguyen, Matthias Weidlich, and Hongzhi Yin. Manipulating recommender systems: A survey of poisoning attacks and countermeasures, 2024. 8
- [41] NYU Journal of Intellectual Property & Entertainment Law. Andersen v. stability ai: The landmark case unpacking the copyright risks of ai image generators. <https://jipel.law.nyu.edu/andersen-v-stability-ai-the-landmark-case-unpacking-the-copyright-risks-of-ai-image-generators/>, 2025. 1
- [42] OpenAI. Chatgpt. <https://chat.openai.com/>, 2025. 1
- [43] Zhuoshi Pan, Yuguang Yao, Gaowen Liu, Bingquan Shen, H. Vicky Zhao, Ramana Rao Kompella, and Sijia Liu. From trojan horses to castle walls: Unveiling bilateral data poisoning effects in diffusion models, 2024. 8
- [44] Yong-Hyun Park, Mingi Kwon, Junghyo Jo, and Youngjung Uh. Unsupervised discovery of semantic latent directions in diffusion models, 2023. 2
- [45] The IP Press. Ghibli ai art and copyright: The dilemma of ghibli-style creations and the looming legal battles ahead. <https://www.theippress.com/2025/03/31/ghibli-ai-art-and-copyright-the-copyright-dilemma-of-ghibli-style-creations-and-the-looming-legal-battles-ahead/>, 2025. 1
- [46] Md. Maklachur Rahman. A DWT, DCT and SVD Based Watermarking Technique to Protect the Image Piracy. *International Journal of Managing Public Sector Information and Communication Technologies*, 4(2):21–32, 2013. 8
- [47] Aditya Ramesh, Prafulla Dhariwal, Alex Nichol, Casey Chu, and Mark Chen. Hierarchical Text-Conditional Image Generation with CLIP Latents, 2022. 1
- [48] Robin Rombach, Andreas Blattmann, Dominik Lorenz, Patrick Esser, and Björn Ommer. High-Resolution Image Synthesis with Latent Diffusion Models, 2022. 1, 8
- [49] Olaf Ronneberger, Philipp Fischer, and Thomas Brox. U-net: Convolutional networks for biomedical image segmentation, 2015. 2
- [50] Nataniel Ruiz, Yuanzhen Li, Varun Jampani, Yael Pritch, Michael Rubinstein, and Kfir Aberman. DreamBooth: Fine Tuning Text-to-Image Diffusion Models for Subject-Driven Generation, 2023. 1
- [51] Anastasiia Safonova, Gohar Ghazaryan, Stefan Stiller, Magdalena Main-Knorn, Claas Nendel, and Masahiro Ryo. Ten deep learning techniques to address small data problems with remote sensing. *International Journal of Applied Earth Observation and Geoinformation*, 125:103569, 2023. 6
- [52] Chitwan Saharia, Jonathan Ho, William Chan, Tim Salimans, David J. Fleet, and Mohammad Norouzi. Image Super-Resolution via Iterative Refinement, 2021. 1
- [53] Chitwan Saharia, William Chan, Saurabh Saxena, Lala Li, Jay Whang, Emily Denton, Seyed Kamyar Seyed Ghasemipour, Burcu Karagol Ayan, S. Sara Mahdavi, Rapha Gontijo Lopes, Tim Salimans, Jonathan Ho, David J Fleet, and Mohammad Norouzi. Photorealistic Text-to-Image Diffusion Models with Deep Language Understanding, 2022. 1
- [54] SAN News. Studio ghibli ai art is going viral but could raise copyright concerns. <https://san.com/cc/studio-ghibli-ai-art-is-going-viral-but-could-raise-copyright-concerns/>, 2025. 1
- [55] Mia Sato. The latest ai copyright lawsuit involves mike huckabee and his books. <https://www.theverge.com/2023/10/19/23924246/mike-huckabee-books-lawsuit-generative-ai-microsoft-meta-bloomberg-eleutherai-books3>, 2023. 1
- [56] Shawn Shan, Wenxin Ding, Josephine Passananti, Stanley Wu, Haitao Zheng, and Ben Y. Zhao. Nightshade: Prompt-Specific Poisoning Attacks on Text-to-Image Generative Models, 2024. 8
- [57] Shawn Shan, Jenna Cryan, Emily Wenger, Haitao Zheng, Rana Hanocka, and Ben Y. Zhao. Glaze: Protecting Artists from Style Mimicry by Text-to-Image Models, 2025. 8
- [58] Shuo Shao, Yiming Li, Hongwei Yao, Yiling He, Zhan Qin, and Kui Ren. Explanation as a watermark: Towards harmless and multi-bit model ownership verification via watermarking feature attribution, 2024. 8
- [59] Jiaming Song, Chenlin Meng, and Stefano Ermon. Denoising Diffusion Implicit Models, 2022. 2
- [60] Yang Song and Stefano Ermon. Generative Modeling by Estimating Gradients of the Data Distribution. In *Advances in Neural Information Processing Systems (NeurIPS)*, 2019.

- [61] Yang Song, Jascha Sohl-Dickstein, Diederik P Kingma, Abhishek Kumar, Stefano Ermon, and Ben Poole. Score-Based Generative Modeling through Stochastic Differential Equations. In *International Conference on Learning Representations (ICLR)*, 2021. 2
- [62] Hui Sun, Tianqing Zhu, Zhiqiu Zhang, Dawei Jin, Ping Xiong, and Wanlei Zhou. Adversarial attacks against deep generative models on data: A survey. *IEEE Transactions on Knowledge and Data Engineering*, 35(4):3367–3388, 2023. 8
- [63] Matthew Tancik, Ben Mildenhall, and Ren Ng. Stegastamp: Invisible hyperlinks in physical photographs, 2020. 8
- [64] The Linux Kernel Developers. BCH Error-Correcting Code Library (lib/bch.c). <https://codebrowser.dev/linux/linux/lib/bch.c.html>, 2024. Implements binary BCH encoding and decoding. Accessed: 2025-10-25. 16
- [65] Patrick von Platen, Suraj Momchev, Valentin De Bortoli, and Thomas Wolf. Diffusers: State-of-the-art diffusion models. <https://github.com/huggingface/diffusers>, 2022. 5, 7, 8
- [66] Zhou Wang, Alan C. Bovik, Hamid R. Sheikh, and Eero P. Simoncelli. Image quality assessment: From error visibility to structural similarity. *IEEE Transactions on Image Processing*, 13(4):600–612, 2004. 5
- [67] Zilan Wang, Junfeng Guo, Jiacheng Zhu, Yiming Li, Heng Huang, Muhao Chen, and Zhengzhong Tu. SleeperMark: Towards Robust Watermark against Fine-Tuning Text-to-image Diffusion Models, 2025. 4, 7, 8
- [68] Washington Journal of Law, Technology & Arts. Studio ghibli-style ai images and the legal questions they raise. <https://wjta.com/2025/04/17/studio-ghibli-style-ai-images-and-the-legal-questions-they-raise/>, 2025. 1
- [69] Yuxin Wen, John Kirchenbauer, Jonas Geiping, and Tom Goldstein. Tree-rings watermarks: Invisible fingerprints for diffusion images. In *Thirty-seventh Conference on Neural Information Processing Systems*, 2023. 2, 8
- [70] Xinting Wu, Ying Huang, Hu Guan, Baoning Niu, Jie Liu, and Shuwu Zhang. Research progress of aigc image watermarking technology based on diffusion model. In *Proceedings of the 2024 10th International Conference on Communication and Information Processing*, page 462–468, New York, NY, USA, 2025. Association for Computing Machinery. 1
- [71] Kevin Alex Zhang, Lei Xu, Alfredo Cuesta-Infante, and Kalyan Veeramachaneni. Robust invisible video watermarking with attention, 2019. 8
- [72] Richard Zhang, Phillip Isola, Alexei A. Efros, Eli Shechtman, and Oliver Wang. The unreasonable effectiveness of deep features as a perceptual metric. In *Proceedings of the IEEE Conference on Computer Vision and Pattern Recognition (CVPR)*, pages 586–595, 2018. 4, 5
- [73] Pinlong Zhao, Weiyao Zhu, Pengfei Jiao, Di Gao, and Ou Wu. Data Poisoning in Deep Learning: A Survey, 2025. 8
- [74] Xuandong Zhao, Kexun Zhang, Zihao Su, Saastha Vasan, Ilya Grishchenko, Christopher Kruegel, Giovanni Vigna, Yu-Xiang Wang, and Lei Li. Invisible image watermarks are provably removable using generative ai, 2024. 2, 8
- [75] Yunqing Zhao, Tianyu Pang, Chao Du, Xiao Yang, Ngai-Man Cheung, and Min Lin. A recipe for watermarking diffusion models. *arXiv preprint arXiv:2303.10137*, 2023. 2, 5, 13

## Appendix

**Overview.** In this supplementary material, we present the following:

<b>A Algorithms</b>	<b>12</b>
<b>B Hyperparameter Configurations for Training and Downstream Finetuning</b>	<b>12</b>
<b>C Additional Results to Section 4.1</b>	<b>13</b>
<b>D Common Distortions in Evaluation</b>	<b>13</b>
<b>E Detailed Evaluation Results of Recipe</b>	<b>13</b>
<b>F LoRA Rank Analysis</b>	<b>14</b>
<b>G Sample Pairs of Original and Watermarked Images</b>	<b>14</b>
<b>H Visual Results as Finetuning on Clean Images versus Finetuning on Watermarked Images</b>	<b>14</b>
<b>I. Tabularized Results on Relationship between HMARK’s Effectiveness and Number of Training Samples</b>	<b>15</b>
<b>J. Tabularized Results on Secret Size Analysis</b>	<b>15</b>
<b>K Tabularized Results on Relationship between Secret Recovery Accuracy and Finetuning</b>	<b>15</b>
<b>L BCH Error Correction Integration</b>	<b>16</b>

### A. Algorithms

We present HMARK’s watermark encoder–decoder training algorithm in Algorithm 1. HMARK’s full pipeline is shown in Algorithm 2.

### B. Hyperparameter Configurations for Training and Downstream Finetuning

The hyperparameters at Stage 1 watermark encoder–decoder training are as follows. The training is conducted with the number of epochs set to 100, batch size set to 16, and learning rate (lr) set to 0.0003. As for the loss function, we set  $\lambda_{\text{wm}} = 5.0$ ,  $\lambda_{\text{secret}} = 3.0$ ,  $\lambda_{\text{image}} = 1.5$ , and  $\lambda_{\text{lpiips}} = 2.0$ . We set the distortion probability  $p_{\text{distort}} = 1.0$ . Finally, the number of secret bits is set to 8, 16, and 32, respectively, based on the specific experimental configurations. The finetuning hyperparameters at Stage 3 are set as follows. By default, for both finetuning scripts, we set resolution to 256, train\_batch\_size to 16, mixed\_precision to “no”, checkpointing\_steps

---

### Algorithm 1 Stage 1 HMARK Training

---

**Input:** Training dataset  $\mathcal{D}$ , encoder  $E_\theta$ , detector  $D_\phi$

**Input:** Loss weights  $\lambda_{\text{wm}}$ ,  $\lambda_{\text{secret}}$ ,  $\lambda_{\text{image}}$ ,  $\lambda_{\text{lpiips}}$

**Output:** Trained encoder  $E_\theta^*$ , detector  $D_\phi^*$

```

1: Initialize  $\theta, \phi$  randomly
2: for epoch = 1 to  $N_{\text{epochs}}$  do
3:   for  $\mathbf{x}$  in  $\mathcal{D}$  do
4:     Sample random secret  $\mathbf{s} \sim \{0, 1\}^B$ 
5:     // Watermark embedding
6:      $\Delta_h, \mathbf{s}_{\text{self}} \leftarrow E_\theta(\mathbf{s})$ 
7:      $\mathbf{x}_{\text{wm}} \leftarrow \text{embed}(\mathbf{x}, \Delta_h)$ 
8:     // Apply random distortion with probability
            $p_{\text{distort}}$ 
9:     if random() <  $p_{\text{distort}}$  then
10:        $\mathbf{x}_{\text{wm}} \leftarrow \text{distort}(\mathbf{x}_{\text{wm}})$ 
11:     end if
12:     // Detection
13:      $p_w, \mathbf{s}_w \leftarrow D_\phi(\mathbf{x}_{\text{wm}})$ 
14:      $p_c, \mathbf{s}_c \leftarrow D_\phi(\mathbf{x})$ 
15:     // Compute losses
16:      $\mathcal{L}_{\text{wm}} = \text{BCE}(p_w, 1) + \text{BCE}(p_c, 0)$ 
17:      $\mathcal{L}_{\text{secret}} = \text{BCE}(\sigma(\mathbf{s}_w), \mathbf{s}) + \text{BCE}(\mathbf{s}_{\text{self}}, \mathbf{s})$ 
18:      $\mathcal{L}_{\text{image}} = \|\mathbf{x}_{\text{wm}} - \mathbf{x}\|_2^2$ 
19:      $\mathcal{L}_{\text{lpiips}} = \text{LPIPS}(\mathbf{x}_{\text{wm}}, \mathbf{x})$ 
20:      $\mathcal{L} = \lambda_{\text{wm}}\mathcal{L}_{\text{wm}} + \lambda_{\text{secret}}\mathcal{L}_{\text{secret}} + \lambda_{\text{image}}\mathcal{L}_{\text{image}} +$ 
            $\lambda_{\text{lpiips}}\mathcal{L}_{\text{lpiips}}$ 
21:     Update  $\theta, \phi$  using  $\nabla\mathcal{L}$ 
22:   end for
23: end for

```

---

to 500, and lr\_warmup\_steps to 500. For LoRA finetuning, we set lr = 0.0001 and rank to 8, 16, or 32 based on the specific experiment; and for the default UNet finetuning, we set lr = 0.0002 with the use\_ema flag set to “True”.

Table 5. Performance of HMARK evaluated on  $\mathcal{D}_{\text{clean}}$  under various distortions when  $\mathcal{M}_{\text{adv}}$  is finetuned on watermark-free  $\mathcal{D}_{\text{orig}}$  using LoRA finetuning (rank = 32).

Distortion	Acc <sub>WM</sub> (%)	Acc <sub>bit</sub> (%)	FPR (%)
Identity	96.0	29.44	4.0
Gaussian Noise	95.5	30.94	4.5
Brightness	96.0	30.0	4.0
Contrast	96.0	30.06	4.0
Blur	93.0	30.0	7.0
JPEG	95.0	29.31	5.0
Resize	86.0	32.12	14.0
<b>Average</b>	<b>93.93</b>	<b>30.27</b>	<b>6.07</b>

---

**Algorithm 2** HMARK Pipeline

---

**Input:** Original dataset  $\mathcal{D}_{\text{orig}}$  owned by dataset owner, suspect DM  $\mathcal{M}_{\text{adv}}$  owned by adversary

- 1: **Stage 1:** Train watermark encoder  $E_\theta$  and detector  $D_\phi$  and produces trained encoder  $E_\theta^*$ , detector  $D_\phi^*$
- 2: **Stage 2:** Dataset owner generates watermarked dataset  $\mathcal{D}_{\text{wm}}$  from  $\mathcal{D}_{\text{orig}}$  with HMARK
- 3: **for**  $\mathbf{x}$  in  $\mathcal{D}_{\text{orig}}$  **do**
- 4:    $\mathbf{s} \leftarrow$  fixed secret pattern with length  $B$ ,  $\mathbf{s} \in \{0, 1\}^B$
- 5:    $\mathbf{x}_{\text{wm}} \leftarrow \text{embed}(\mathbf{x}, E_\theta^*(\mathbf{s}))$
- 6:   Save  $\mathbf{x}_{\text{wm}}$  to  $\mathcal{D}_{\text{wm}}$
- 7: **end for**
- 8: **Stage 3:** Adversary finetunes downstream DM  $\mathcal{M}_{\text{adv}}$
- 9:  $\mathcal{M}_{\text{adv}} \leftarrow \text{finetune}(\mathcal{M}_{\text{adv}}, \mathcal{D}_{\text{wm}})$
- 10: **Stage 4:** Dataset owner verifies IP infringement and test radioactivity
- 11: **for**  $i = 1$  to  $N_{\text{test}}$  **do**
- 12:    $\mathcal{D}_{\text{adv}} \leftarrow \mathcal{M}_{\text{adv}}.\text{generate}()$
- 13:    $p_{\text{detect}}, \mathbf{s}_{\text{pred}} \leftarrow D_\phi^*(\mathcal{D}_{\text{adv}})$
- 14:   Record watermark detection rate and secret accuracy
- 15: **end for**

---

### C. Additional Results to Section 4.1

Table 5 records HMARK’s watermark detection when  $\mathcal{M}_{\text{adv}}$  is LoRA finetuned on samples from  $\mathcal{D}_{\text{orig}}$  (*i.e.*, all of them should be True Negatives). 93.93%  $\text{Acc}_{\text{WM}}$  means that HMARK correctly identifies 93.93% of the images as non-watermarked and 6.07% of them are incorrectly identified as watermarked.  $\text{Acc}_{\text{bit}}$  being 30.27% means that HMARK cannot extract the correct majority of the watermark’s bits from  $\mathcal{M}_{\text{adv}}$ ’s generated outputs, which is the expected behavior.

Table 6. Performance of HMARK evaluated on watermarked images ( $\mathcal{D}_{\text{wm}}$ ) generated at Stage 2 under different distortion types.

Distortion	$\text{Acc}_{\text{WM}}$ (%)	$\text{Acc}_{\text{bit}}$ (%)	P (%)	R (%)	F1 (%)
Identity	99.8	97.2	99.6	100	99.8
Blur	97.6	98.0	95.4	100	97.7
Noise	99.8	98.5	99.6	100	99.8
JPEG	99.8	97.2	99.6	100	99.8
Brightness	99.8	96.3	99.6	100	99.8
Contrast	99.8	96.5	99.6	100	99.8
Resize	96.6	98.1	93.6	100	96.7
<b>Average</b>	<b>99.0</b>	<b>97.4</b>	<b>98.1</b>	<b>100.0</b>	<b>99.1</b>

### D. Common Distortions in Evaluation

As discussed in Section 4.2, we evaluate the resistance of our watermarking scheme against a wide range of distortions. For blur perturbations, we use Gaussian kernels with standard deviations ranging from 0.3 to 0.8. Additive Gaussian noise is introduced with standard deviations ranging between

Table 7. Performance of HMARK evaluated on downstream DDPM’s generated outputs ( $\mathcal{D}_{\text{adv}}$ ) at Stage 4 under different distortions. The DDPM is trained with the default UNet finetuning.

Distortion	$\text{Acc}_{\text{WM}}$ (%)	$\text{Acc}_{\text{bit}}$ (%)	P (%)	R (%)	F1 (%)
Identity	99.5	84.4	99.0	100	99.5
Gaussian Noise	98.5	85.5	97.1	100	98.5
Brightness	99.0	84.3	98.0	100	99.0
Contrast	99.5	85.1	99.0	100	99.5
Blur	98.5	86.3	97.1	100	98.5
JPEG	99.0	85.4	98.0	100	99.0
Resize	98.5	87.3	97.1	100	98.5
<b>Average</b>	<b>98.93</b>	<b>85.2</b>	<b>97.9</b>	<b>100</b>	<b>98.9</b>

0.005 and 0.02, while JPEG-like compression artifacts are simulated using random multiplicative noise factors in the range of 0.01–0.12. Spatial distortions are tested by resizing images with scale factors from 0.85 to 0.95, followed by bilinear interpolation back to the original resolution. Photometric perturbations such as brightness and contrast are adjusted with random multiplicative factors sampled from 0.9–1.1. These perturbations simulate the types of degradations that commonly occur in real-world imaging pipelines, enabling a systematic evaluation of the model’s resistance to visual noise and distortions.

Table 6 presents HMARK’s watermark embedding performance and resistance to distortions at Stage 2, directly after watermark embedding. Table 7 records the performance of HMARK when the finetuning script is the default UNet, complementary to Table 2 where the finetuning script is LoRA with  $\text{rank} = 32$ .

Table 8. Performance of Recipe evaluated on watermarked images at Stage 2 under different distortion types.

Distortion	$\text{Acc}_{\text{WM}}$ (%)	$\text{Acc}_{\text{bit}}$ (%)	P (%)	R (%)	F1 (%)
Identity	99.4	57.0	98.8	100	99.4
Gaussian Noise	99.2	57.0	98.5	100	99.3
Brightness	99.0	57.5	98.0	100	99.0
Contrast	99.2	57.3	98.4	100	99.2
Blur	99.4	57.0	98.8	100	99.4
JPEG	99.2	57.6	98.3	100	99.2
Resize	99.4	57.0	98.8	100	99.4
<b>Average</b>	<b>99.26</b>	<b>57.2</b>	<b>98.5</b>	<b>100</b>	<b>99.27</b>

### E. Detailed Evaluation Results of Recipe

Complementary to Section 4.1, we present the baseline competitor Recipe’s [75] performance at Stage 2 in Table 8 and its performance at Stage 4 in Table 9 for default UNet finetuning and Table 10 for LoRA finetuning.

Table 9. Performance of Recipe evaluated on downstream DDPM’s generated outputs at Stage 4 under different distortion types. The DDPM is trained with the default UNet finetuning script.

Distortion	Acc <sub>WM</sub> (%)	Acc <sub>bit</sub> (%)	P (%)	R (%)	F1 (%)
Identity	50.5	15.9	66.7	2.0	3.9
Gaussian Noise	51.0	16.0	100.0	2.0	3.9
Brightness	51.5	18.4	80.0	4.0	7.6
Contrast	51.0	17.9	66.7	4.0	7.5
Blur	50.5	15.8	66.7	2.0	3.9
JPEG	50.5	17.2	60.0	3.0	5.7
Resize	50.5	15.9	66.7	2.0	3.9
<b>Average</b>	<b>50.79</b>	<b>16.73</b>	<b>72.4</b>	<b>2.71</b>	<b>5.2</b>

Table 10. Performance of Recipe evaluated on downstream DDPM’s generated outputs at Stage 4 under different distortion types. The DDPM is trained with LoRA finetuning script.

Distortion	Acc <sub>WM</sub> (%)	Acc <sub>bit</sub> (%)	P (%)	R (%)	F1 (%)
Identity	50.5	15.9	66.7	2.0	3.9
Gaussian Noise	49.5	16.2	40.0	2.0	3.8
Brightness	51.0	15.3	100.0	2.0	3.9
Contrast	51.0	15.1	100.0	2.0	3.9
Blur	51.0	15.7	100.0	2.0	3.9
JPEG	50.5	18.5	66.7	2.0	3.9
Resize	50.5	15.9	66.7	2.0	3.9
<b>Average</b>	<b>50.57</b>	<b>16.09</b>	<b>77.16</b>	<b>2.00</b>	<b>3.89</b>

Table 11. Performance of HMARK when downstream DDPM finetunes using LoRA with different ranks at step 9,000 and 8-bit secret size.

Rank	Acc <sub>WM</sub> (%)	Acc <sub>bit</sub> (%)	P (%)	R (%)	F1 (%)
8	98.29	89.29	97.34	99.29	98.30
16	98.14	91.14	97.20	99.14	98.16
32	98.57	95.07	97.22	100.00	98.59

Table 12. Performance of HMARK evaluated on downstream DDPM’s generated outputs ( $\mathcal{D}_{adv}$ ) at Stage 4 under different distortion types. The DDPM is trained with the LoRA finetuning script ( $\text{rank} = 16$ ). Secret bit size is 8.

Distortion	Acc <sub>WM</sub> (%)	Acc <sub>bit</sub> (%)	P (%)	R (%)	F1 (%)
Identity	98.50	89.12	98.02	99.00	98.51
Gaussian Noise	98.00	92.88	97.06	99.00	98.02
Brightness	98.50	90.00	98.02	99.00	98.51
Contrast	98.50	88.75	98.02	99.00	98.51
Blur	98.50	92.50	98.02	99.00	98.51
JPEG	99.00	91.12	98.04	100.00	99.01
Resize	96.00	94.62	93.40	99.00	96.12
<b>Average</b>	<b>98.14</b>	<b>91.14</b>	<b>97.20</b>	<b>99.14</b>	<b>98.16</b>

Table 13. Performance of HMARK evaluated on downstream DDPM’s generated outputs at Stage 4 under different distortion types. The DDPM is trained with the LoRA finetuning script ( $\text{rank} = 8$ ). Secret bit size is 8.

Distortion	Acc <sub>WM</sub> (%)	Acc <sub>bit</sub> (%)	P (%)	R (%)	F1 (%)
Identity	98.5	87.62	98.02	99.00	98.51
Gaussian Noise	99.0	88.75	98.04	100.00	99.01
Brightness	98.0	87.38	97.06	99.00	98.02
Contrast	98.5	87.00	98.02	99.00	98.51
Blur	98.5	92.12	98.02	99.00	98.51
JPEG	98.5	88.62	98.02	99.00	98.51
Resize	97.0	94.75	94.34	100.00	97.09
<b>Average</b>	<b>98.29</b>	<b>89.29</b>	<b>97.34</b>	<b>99.29</b>	<b>98.30</b>

## F. LoRA Rank Analysis

Table 11 shows the comparison of HMARK’s performance at Stage 4 when finetuned for 9,000 steps using LoRA with different ranks (32, 16, 8). Detailed results on resistance to distortions are presented in Tables 2, 12, and 13. While Acc<sub>WM</sub> for all tested LoRA ranks are similar (*i.e.*, above 98%), a higher LoRA rank leads to a higher Acc<sub>bit</sub>. However, it is worth noting that Acc<sub>bit</sub> for all tested ranks reach 94.50% eventually with further finetuning (See Table 18).

## G. Sample Pairs of Original and Watermarked Images

We present additional pairs of original and watermarked images generated by HMARK in Figure 5.

## H. Visual Results as Finetuning on Clean Images versus Finetuning on Watermarked Images

Figure 6 shows the comparison of semantic shifts and visual quality of  $\mathcal{D}_{clean}$  and  $\mathcal{D}_{adv}$  generated by  $\mathcal{M}_{adv}$  LoRA-finetuned on 10k clean ( $\mathcal{D}_{orig}$ ), 8-bit, 16-bit, and 32-bit secret embedded watermarked data samples ( $\mathcal{D}_{wm}$ ).

Table 14. Impact of the size of  $\mathcal{D}_{wm}$  acquired by the adversary to finetune  $\mathcal{M}_{adv}$  on HMARK’s performance.  $\mathcal{M}_{adv}$  is LoRA ( $\text{rank} = 32$ ) finetuned on  $\mathcal{D}_{wm}$  with an 8-bit secret embedded.

$ \mathcal{D}_{wm} $	Acc <sub>WM</sub> (%)	Acc <sub>bit</sub> (%)	P (%)	R (%)	F1 (%)
1,000	98.57	97.29	97.22	100	98.59
3,000	98.64	97.29	97.36	100	98.66
5,000	98.50	94.86	97.22	99.86	98.52
7,000	98.43	94.21	97.08	99.86	98.45
10,000	98.57	95.07	97.22	100	98.59
15,000	98.57	95.43	97.22	100	98.59
20,000	98.57	96.43	97.22	100	98.59

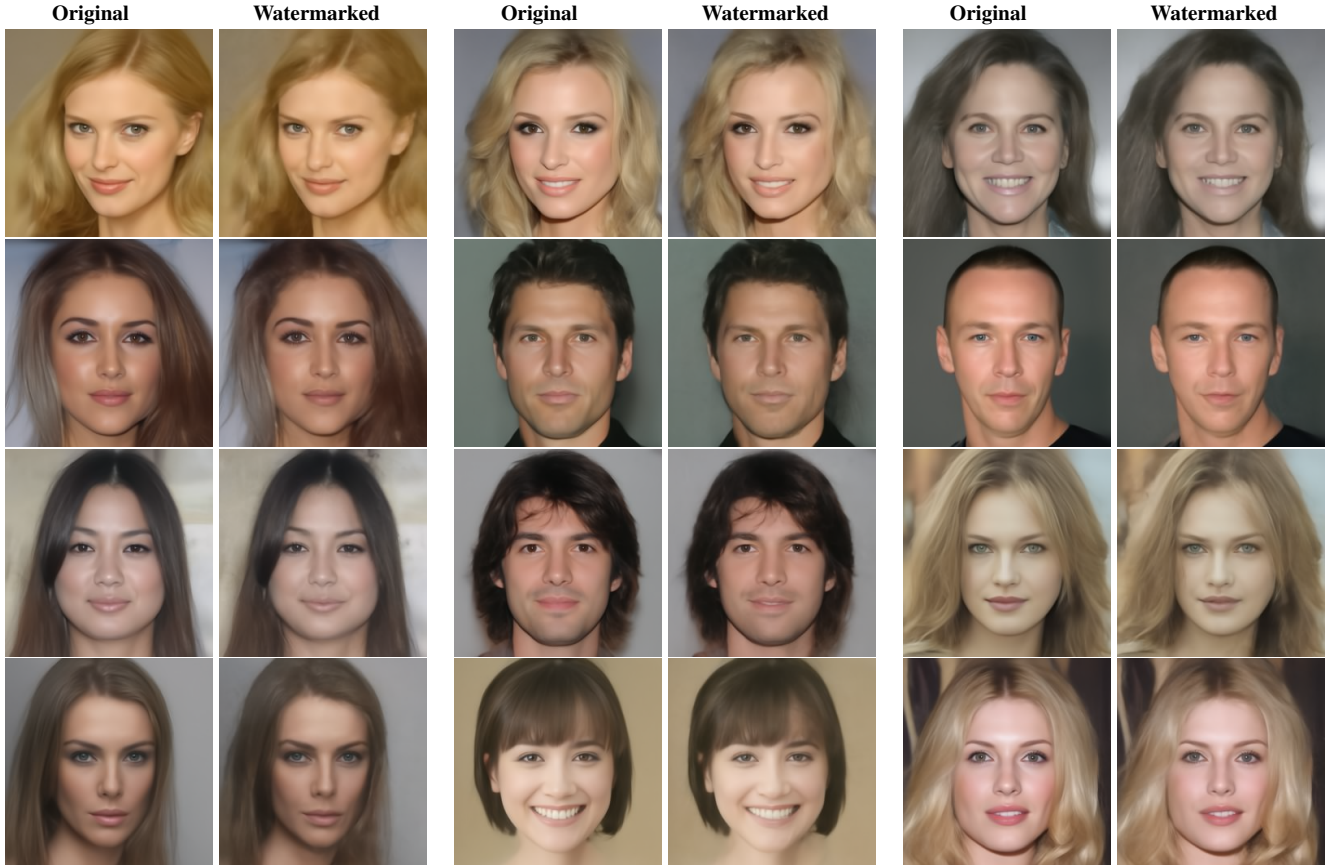


Figure 5. Visual comparison between original and watermarked images across multiple samples. Each pair shows the original (left) and its corresponding watermarked (right) image.

Table 15. HMARK’s radioactivity performance on downstream DDPM  $\mathcal{M}_{adv}$  finetuned with the default UNet script using different secret bit lengths.

# Bits	Acc <sub>WM</sub> (%)	Acc <sub>bit</sub> (%)	P (%)	R (%)	F1 (%)
8	98.14	87.43	97.33	99.00	98.16
16	99.21	78.93	98.45	100	99.22
32	93.50	68.50	88.50	100	93.90

### I. Tabularized Results on Relationship between HMARK’s Effectiveness and Number of Training Samples

Table 14 shows the detailed performance of HMARK with different  $\mathcal{D}_{wm}$  sizes, which is complementary to the discussion in Section 4.1.

### J. Tabularized Results on Secret Size Analysis

As Table 4 in Section 4.4 presents, LoRA has higher Acc<sub>bit</sub> as we increase the secret size. It achieves above 93% Acc<sub>bit</sub> when the secret size is less than 32 bits and drops to 68%

when 32 bits are embedded. Table 15 shows the average radioactivity performance of HMARK when  $\mathcal{M}_{adv}$  is finetuned with the default UNet script. Table 16 illustrates the effectiveness of HMARK in detail when embedding 8-bit, 16-bit, and 32-bit secrets and finetuning using the default UNet script and LoRA. The results match the intuition discussed in Section 3.4 that as more bits are transmitted during downstream finetuning, Acc<sub>bit</sub> drops gracefully. This motivates the integration of error correction compatibility in our tool (See Appendix L).

### K. Tabularized Results on Relationship between Secret Recovery Accuracy and Finetuning

Tables 17 and 18 show how HMARK’s performance evolves across downstream DDPM finetuning steps using the default finetuning script and LoRA. When  $\mathcal{M}_{adv}$  is finetuned with the default UNet finetuning script, the trend matches the discussion about LoRA finetuning in Section 4.5. At the early stages (1k–3k steps), the Acc<sub>bit</sub> is relatively low (61–63%), indicating that the watermark signal has not yet fully stabi-

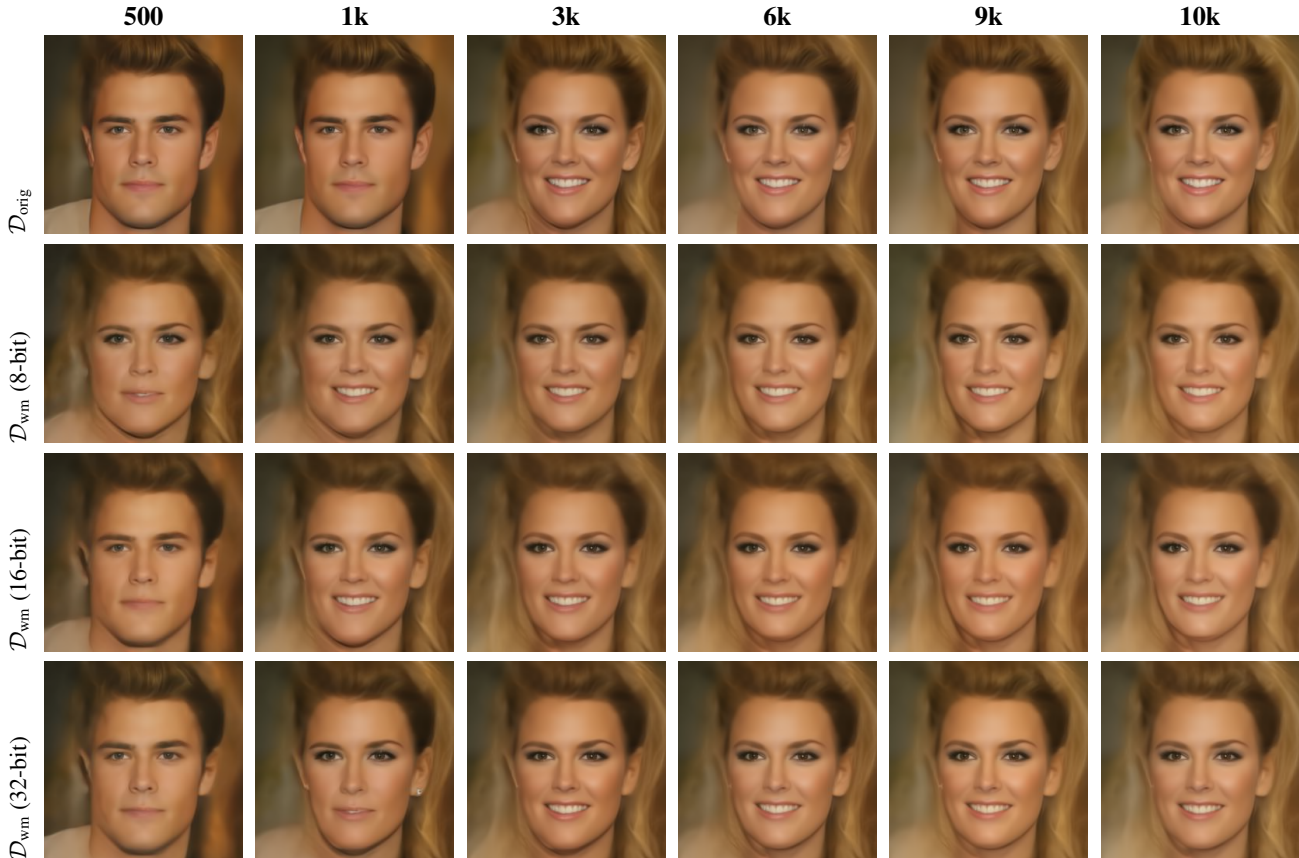


Figure 6. Comparison of generations from  $\mathcal{M}_{adv}$  finetuned with LoRA ( $\text{rank} = 32$ ) across finetuning steps when trained on (top)  $\mathcal{D}_{orig}$ , (second)  $\mathcal{D}_{wm}$  with 8-bit secret, (third)  $\mathcal{D}_{wm}$  with 16-bit secret, and (bottom)  $\mathcal{D}_{wm}$  with 32-bit secret.

lized. As default UNet finetuning progresses, both overall accuracy and secret accuracy steadily improve, reaching over 85% after 6k steps and exceeding 87% by 30k steps, which matches our theoretical intuition in Section 3.4. Precision, recall, and F1 remain consistently high throughout, suggesting that the watermark detector remains reliable. These results demonstrate that a moderate number of finetuning iterations (6k-9k steps) is sufficient for convergence and high watermark recovery for both finetuning scripts.

## L. BCH Error Correction Integration

Motivated by the observations in the relationship between secret size and  $\text{Acc}_{bit}$  when  $\mathcal{M}_{adv}$  is finetuned on the default UNet finetuning script with limited finetuning steps, HMARK also supports Bose-Chaudhuri-Hocquenghem (BCH) error correction code (ECC) [2] to produce codewords  $\mathbf{s}_{ecc} \in \{0, 1\}^n$  with error correction capabilities. Specifically, the  $\text{BCH}(n, k)$  encoding scheme allows the system to transmit parity bits to recover lost messages, where  $n$  is the total codeword length and  $k$  denotes the number of secret data bits. When ECC mode is enabled, the encoder  $E_\theta$  operates on BCH-encoded secrets instead of

raw  $k$ -bit secret vectors, while the detector adapts to predict  $n$ -bit codewords. During inference, the predicted codeword is BCH-decoded to reconstruct the original  $k$ -bit message. We implement BCH using `bchlib` [27], which wraps the Linux kernel BCH library [64]. The implementation constrains the Galois field order to  $m \in [5, 15]$ , corresponding to codeword lengths  $n = 2^m - 1$  and setting the smallest supported  $n$  to 31. In practice, both  $\text{BCH}(31, 8)$  and  $\text{BCH}(31, 16)$  substantially improve robustness, increasing  $\text{Acc}_{bit}$  beyond 90% under downstream DM finetuning. Apart from Table 19, which shows the comparison of HMARK’s performance with and without BCH error correction, Tables 20 and 21 show the detailed performance of HMARK under various distortions when BCH is integrated. We draw the conclusion that BCH helps improve  $\text{Acc}_{bit}$  to above 90% even when more secret bits are embedded and transmitted.

Table 16. Performance of HMARK evaluated on downstream DDPM ( $\mathcal{M}_{\text{adv}}$ )’s generated outputs ( $\mathcal{D}_{\text{adv}}$ ) at Stage 4 under different finetuning scripts (UNet vs. LoRA) and bit configurations. The results are collected at the finetuning step 9,000.

Finetuning Script	# Bits	Distortion	Acc <sub>WM</sub> (%)	Acc <sub>bit</sub> (%)	P (%)	R (%)	F1 (%)
UNet	8	Identity	99.5	84.4	99.0	100	99.5
		Gaussian Noise	98.5	85.5	97.1	100	98.5
		Brightness	99.0	84.3	98.0	100	99.0
		Contrast	99.5	85.1	99.0	100	99.5
		Blur	98.5	86.3	97.1	100	98.5
		JPEG	99.0	85.4	98.0	100	99.0
		Resize	98.5	87.3	97.1	100	98.5
		<b>Average</b>	<b>98.93</b>	<b>85.2</b>	<b>97.9</b>	<b>100</b>	<b>98.9</b>
	16	Identity	99.5	78.50	99.01	100.00	99.50
		Gaussian Noise	99.5	80.12	99.01	100.00	99.50
		Brightness	99.5	77.25	99.01	100.00	99.50
		Contrast	99.5	80.12	99.01	100.00	99.50
		Blur	99.0	78.75	98.04	100.00	99.01
		JPEG	99.5	79.94	99.01	100.00	99.50
		Resize	98.0	79.12	96.15	100.00	98.04
		<b>Average</b>	<b>99.21</b>	<b>78.93</b>	<b>98.45</b>	<b>100.00</b>	<b>99.22</b>
	32	Identity	93.5	68.38	91.43	96.00	93.66
		Gaussian Noise	91.5	68.34	88.79	95.00	91.79
		Brightness	93.5	68.22	93.07	94.00	93.53
		Contrast	92.0	68.44	89.62	95.00	92.23
		Blur	89.5	68.41	84.96	96.00	90.14
		JPEG	92.0	68.34	89.62	95.00	92.23
		Resize	86.5	68.44	80.17	97.00	87.78
		<b>Average</b>	<b>91.21</b>	<b>68.00</b>	<b>88.01</b>	<b>95.43</b>	<b>91.57</b>
LoRA (rank = 32)	8	Identity	99.00	94.00	98.04	100.00	99.01
		Gaussian Noise	99.00	95.75	98.04	100.00	99.01
		Brightness	98.50	94.38	97.09	100.00	98.52
		Contrast	99.00	94.50	98.04	100.00	99.01
		Blur	98.50	95.50	97.09	100.00	98.52
		JPEG	99.00	95.25	98.04	100.00	99.01
		Resize	97.00	97.12	94.34	100.00	97.09
		<b>Average</b>	<b>98.57</b>	<b>95.07</b>	<b>97.22</b>	<b>100.00</b>	<b>98.59</b>
	16	Identity	99.5	92.88	100.00	99.00	99.50
		Gaussian Noise	99.5	94.12	100.00	99.00	99.50
		Brightness	100.0	93.94	100.00	100.00	100.00
		Contrast	99.5	93.50	100.00	99.00	99.50
		Blur	99.5	93.81	100.00	99.00	99.50
		JPEG	100.0	93.81	100.00	100.00	100.00
		Resize	98.5	94.00	98.02	99.00	98.51
		<b>Average</b>	<b>99.50</b>	<b>93.73</b>	<b>99.43</b>	<b>99.14</b>	<b>99.50</b>
	32	Identity	91.0	68.81	89.42	93.00	91.18
		Gaussian Noise	92.0	68.72	89.62	95.00	92.23
		Brightness	91.0	68.59	89.42	93.00	91.18
		Contrast	89.0	68.53	87.50	91.00	89.22
		Blur	90.5	68.78	85.84	97.00	91.08
		JPEG	92.5	68.69	89.72	96.00	92.75
		Resize	89.0	68.78	83.62	97.00	89.81
		<b>Average</b>	<b>90.71</b>	<b>68.70</b>	<b>87.88</b>	<b>94.57</b>	<b>91.04</b>

Table 17. Performance of HMARK at different finetuning steps when  $\mathcal{M}_{adv}$  is finetuned with default UNet finetuning script.

Steps	Acc <sub>WM</sub> (%)	Acc <sub>bit</sub> (%)	P (%)	R (%)	F1 (%)
1,000	97.79	62.86	97.85	97.71	97.78
3,000	97.00	61.14	97.82	96.14	96.97
5,000	98.50	81.86	97.88	99.14	98.51
6,000	98.93	85.21	97.90	100.00	98.94
9,000	98.14	87.43	97.33	99.00	98.16
10,000	98.57	86.43	98.02	99.14	98.58
20,000	98.50	86.79	98.02	99.00	98.51
30,000	99.00	87.64	98.04	100.00	99.01

Table 18. Performance of HMARK at different finetuning steps when  $\mathcal{M}_{adv}$  is LoRA-finetuned (ranks = 32, 16, 8).

Rank	Steps	Acc <sub>WM</sub> (%)	Acc <sub>bit</sub> (%)	P (%)	R (%)	F1 (%)	
32	500	94.21	50.07	96.82	91.43	94.05	
	1,000	96.64	65.71	97.11	96.14	96.63	
	2,000	97.57	83.71	97.03	98.14	97.59	
	3,000	97.93	86.36	97.19	98.71	97.94	
	5,000	98.43	90.71	97.08	99.86	98.45	
	6,000	98.50	90.86	97.09	100.00	98.52	
	9,000	98.57	95.07	97.22	100.00	98.59	
	10,000	98.57	94.50	97.22	100.00	98.59	
	16	500	83.29	22.07	96.23	69.29	80.56
		1,000	93.43	44.64	96.91	89.71	93.18
2,000		97.00	70.79	97.27	96.71	96.99	
3,000		97.64	78.29	97.30	98.00	97.65	
5,000		98.00	84.93	97.32	98.71	98.01	
6,000		97.79	87.50	97.31	98.29	97.80	
9,000		98.14	91.14	97.20	99.14	98.16	
10,000		98.64	91.93	97.36	100.00	98.66	
30,000		98.43	95.64	97.35	99.57	98.45	
8		500	90.36	35.21	96.85	83.43	89.64
	1,000	95.57	57.14	97.19	93.86	95.49	
	2,000	98.07	79.36	97.19	99.00	98.09	
	3,000	97.79	81.93	97.05	98.57	97.80	
	5,000	98.43	85.57	97.21	99.71	98.45	
	6,000	98.43	89.50	97.35	99.57	98.45	
	9,000	98.29	89.29	97.34	99.29	98.30	
	10,000	98.57	94.50	97.35	99.86	98.59	

Table 19. Comparison of HMARK performance on radioactivity to  $\mathcal{M}_{adv}$  with and without ECC for different watermark secret bit lengths.  $\mathcal{M}_{adv}$  finetuned with the default UNet finetuning script.

ECC	# Total	# Sec.	Acc <sub>WM</sub> (%)	Acc <sub>bit</sub> (%)	P (%)	R (%)	F1 (%)
None	8	8	98.14	87.43	97.33	99.00	98.16
BCH(31, 8)	31	8	97.93	91.14	96.53	99.43	97.96
None	16	16	99.21	78.93	98.45	100.00	99.22
BCH(31, 16)	31	16	99.43	93.02	99.01	99.86	99.43

Table 20. Performance of HMARK evaluated on  $\mathcal{M}_{adv}$ 's generated outputs at Stage 4 using **BCH(31, 8)** ECC under different distortions.  $\mathcal{M}_{adv}$  is finetuned with default UNet finetuning script.

Distortion	Acc <sub>WM</sub> (%)	Acc <sub>bit</sub> (%)	P (%)	R (%)	F1 (%)
Identity	98.5	89.88	98.02	99.00	98.51
Gaussian Noise	98.0	92.75	97.06	99.00	98.02
Brightness	99.5	88.88	99.01	100.00	99.50
Contrast	99.0	89.75	99.00	99.00	99.00
Blur	97.5	92.12	95.24	100.00	97.56
JPEG	98.0	92.62	97.06	99.00	98.02
Resize	95.0	93.50	90.91	100.00	95.24
<b>Average</b>	<b>97.93</b>	<b>91.14</b>	<b>96.53</b>	<b>99.43</b>	<b>97.96</b>

Table 21. Performance of HMARK evaluated on  $\mathcal{M}_{adv}$ 's generated outputs at Stage 4 using **BCH(31, 16)** ECC under different distortions.  $\mathcal{M}_{adv}$  is finetuned with the default UNet finetuning script.

Distortion	Acc <sub>WM</sub> (%)	Acc <sub>bit</sub> (%)	P (%)	R (%)	F1 (%)
Identity	99.5	90.88	99.01	100.00	99.50
Blur	99.5	93.19	99.01	100.00	99.50
Noise	99.0	92.31	99.00	99.00	99.00
JPEG	99.5	93.06	99.01	100.00	99.50
Brightness	100.0	94.06	100.00	100.00	100.00
Contrast	99.5	93.12	99.01	100.00	99.50
Resize	99.0	94.50	98.04	100.00	99.01
<b>Average</b>	<b>99.43</b>	<b>93.02</b>	<b>99.01</b>	<b>99.86</b>	<b>99.43</b>